HHS Public Access

Author manuscript

Oncogene. Author manuscript; available in PMC 2020 October 25.

Published in final edited form as:

Oncogene. 2020 May ; 39(22): 4344–4357. doi:10.1038/s41388-020-1300-x.

Combination of CHEK1/2 Inhibition and Ionizing Radiation Results in Abscopal Tumor Response through Increased Micronuclei Formation

Hann-Hsiang Chao, MD, PhD[1,2,*], **Ilias V. Karagounis, PhD**[1,*], **Christoforos Thomas, PhD**[1], **Noëlle B. François**[1], **Andrea Facciabene, PhD**[1], **Constantinos Koumenis, PhD**[1], **Amit Maity, MD, PhD**[1]

[1]Department of Radiation Oncology, University of Pennsylvania, Philadelphia, PA, USA

[2]Department of Radiation Oncology, McGuire VA Medical Center, Richmond, VA, USA

Abstract

We explore a novel strategy of activating immune signaling through increased micronuclei formation utilizing a cell cycle checkpoint inhibitor to drive cell cycle progression following ionizing radiation. The Chk1/2 inhibitor AZD7762 is used to abrogate radiation therapy (RT)-induced G2/M cell cycle arrest in multiple cell lines and, we find that this therapeutic combination promotes increased micronuclei formation *in vitro* and subsequently drives increased type I interferon signaling and cytotoxic T-cell activation. *In vivo* studies using B16-F10 melanoma cancer cells implanted in C57/BL6 mice demonstrate improved rates of tumor control at the abscopal (unirradiated) site, located outside of the radiation field, only in the AZD7762+RT group, with a corresponding reduction in mean tumor volume, increase in the CD8 T-cell population, and immune activated gene signaling. Our results demonstrate that targeted inhibition of cell cycle checkpoint activation following ionizing radiation drives increased production of immunogenic micronuclei, leading to systemic tumor response with potential future clinical benefit.

Address correspondence to: Amit Maity, MD, PhD, Professor of Radiation Oncology, University of Pennsylvania School of Medicine, Department of Radiation Oncology, TRC 2-West, 3400 Civic Center Boulevard, Philadelphia, PA 19104, Phone: (215) 662-3759, Fax: (215) 349-8975, Amit.Maity@uphs.upenn.edu.

*These authors contributed equally to this work

Authors' Contributions

Conception and design: H. Chao, I. Karagounis, C. Thomas, A. Maity

Development of methodology: H. Chao, I. Karagounis, C. Thomas, A. Facciabene, C. Koumenis, A. Maity

Acquisition of data (provided animals, acquired and managed patients, provided facilities, etc.): H. Chao, I. Karagounis, C. Thomas, N. François

Analysis and interpretation of data (e.g., statistical analysis, biostatistics, computational analysis): H. Chao, I. Karagounis

Writing, review, and/or revision of the manuscript: H. Chao, I. Karagounis, C. Thomas, N. François, A. Facciabene, C. Koumenis, A. Maity

Administrative, technical, or material support (i.e., reporting or organizing data, constructing databases): H. Chao, I. Karagounis, N. François

Study supervision: A. Maity

Competing Interests Statement

A. Maity reports receiving research funding from Merck. No potential competing interests are reported by the other authors.

Keywords

Chk1; Chk2; radiation; micronuclei; immune signaling; abscopal response

Introduction

In anticancer therapeutic treatments, the advent of immunomodulatory agents, has led to improved responses in many disease sites, with many patients achieving long-lasting tumor remissions [3, 4, 29] even in the setting of pre-existing metastatic disease [12, 30, 32]. However, the majority of patients exhibit brief or no response to these agents, driving the search for improved or alternate therapeutic strategies. Recent studies have identified a link between genotoxic cancer treatments and inflammatory gene expression through the generation of micronuclei following DNA damage[16, 23]. Micronuclei can be formed when cells with DNA double-strand breaks are progressing through mitosis or when chromosomal mis-segregation lead to deposition of DNA in the cytosol. This cytosolic DNA can be recognized by sensing proteins such as cyclic GMP-AMP synthase (cGAS) [6, 10, 23, 40]. cGAS localization to micronuclei ultimately drives inflammatory cytokine signaling capable of recruiting immune cells and is essential for local and systemic (abscopal) tumor responses to ionizing radiation, by cGAS activating the interferon gene (STING) pathway [8, 33, 40, 41].

These prior studies additionally found that abscopal tumor regression occurring when ionizing radiation is combined with immune checkpoint blockade *in vivo* is prevented when mitotic progression is impaired and also when cGAS-STING mediated signaling is blocked [11, 16]. We hypothesized that by driving mitotic progression in the context of DNA damage induced by ionizing radiation, the converse effect might be seen. This would in theory result in increased micronuclei formation, increased inflammatory and immune stimulatory signaling, increased anti-tumor innate immune activity, and local and systemic tumor responses. Cell cycle checkpoint activation is typically upregulated following DNA damage, such as that induced by ionizing radiation, which functions to stall mitotic progression and allow for DNA repair [2, 5, 20, 38, 39, 42]. By targeting components of the cell cycle checkpoint, including the serine/threonine kinases Checkpoint 1 and 2 (Chk1/2), mitotic progression can be restored in the setting of radiation-induced DNA damage[45]. Following this line of reasoning, the use of Chk1/2 inhibitors combined with ionizing radiation could lead not only to radiosensitization, but also increased micronuclei formation, driving downstream immune signaling.

Based on prior literature, the compound AZD7762 functions as a Chk1/2 inhibitor and is an effective radiosensitizer[22, 27, 43]. We conducted *in vitro* and *in vivo* analysis combining ionizing radiation with AZD7762. We demonstrate that combination treatment leads to increased cGAS-driven immune signaling through localization of cGAS with micronuclei *in vitro,* an increased CD8 population, and a systemic tumor response *in vivo*.

Materials and Methods

Cell lines, tissue culture and transfections

MCF10A cells, a human mammary epithelial non-tumorigenic cell line, were obtained from ATCC (ATCC Cat# CRL-10317, RRID:CVCL_0598) and cultured at 37 °C in DMEM media 5% fetal bovine serum (FBS) (Gibco), 20ng/mL human EGF (Sigma), 0.5 mg/mL hydrocortisone, and 10 ug/mL human insulin (Sigma). B16-F10 cells, a mouse skin melanoma line with tumorigenic properties, were obtained from ATCC (ATCC Cat# CRL-6475, RRID:CVCL_0159) and cultured at 37 °C in DMEM with 10% FBS and 1% Penicillin/Streptomycin. Both H460, a human large cell carcinoma cell line (ATCC Cat# HBT-177, RRID:CVCL_0459) and H1299, a human non-small cell lung carcinoma cell line (ATCC Cat# CRL-5803, RRID:CVCL_0060) were obtained from ATCC and cultured in DMEM media supplemented with 10% FBS and 1% Penicillin/Streptomycin. All cell lines were maintained and cultured in a humidified incubator at 37°C, 5%CO2. The pLVX-mCherry-cGAS construct was kindly provided by the Roger A. Greenberg (University of Pennsylvania)[16]. MCF10A cells were infected with lentivirus containing the pLVX-mCherry-cGAS plasmid and infected cells were selected with puromycin as described previously[35].

Irradiation and cell treatments

The Chk1/2 inhibitor (AZD7762, Selleck Chemicals) was added 1 hour prior to radiation treatment. The concentration of AZD7762 (25 nM) was chosen based on the lower end of previously published dose ranges in order to limit potential drug toxicity[43]. MCF10A cells received 16 Gy of radiation unless otherwise specified. All other cell lines received 4 Gy of radiation unless otherwise specified. Radiation doses were selected based on prior radiation studies with these cell lines[16, 36] and adjusted as needed to allow for continued proliferation. Specifically, a lower dose was used for the non-MCF10A cell lines as previous experience showed that the 16 Gy dose used in the literature for MCF10A cells was incompatible with survival in the tumor cell lines. The inhibitor was removed 1 day following radiation and media was changed every 2–3 days afterwards. Irradiation was performed under ambient conditions using an X-Rad 320IX at a dose rate of 2.67 Gy/minute.

Flow cytometry

Cell cycle analysis was performed on cells collected from single wells of a six-well tissue culture plate using 0.25% trypsin and washed in PBS prior to fixation with ice-cold 70% ethanol and stored at −20 °C for at least 8 hours. Following fixation, cells were again washed in PBS and then re-suspended in a solution of PBS containing 50 ug/mL propidium iodide (Life Technologies), and 100 ug/mL RNase A (Roche). For flow cytometry analysis of CD8+ T cells, tumors were minced in 2mg/ml collagenase IV followed by a 1-hour incubation at 37°C and then passed through a 70μm cell strainer, washed and pellet. Cells (1×10^6) were then incubated with purified anti-mouse CD16/32 (Biolegend) and subsequently stained with the following monoclonal antibodies against mouse markers: eFluor 450-conjugated anti-mouse CD45 (clone 30-F11, eBioscience), eFluor 506-conjugated anti mouse CD3 (clone 17A2, eBioscience), FITC-conjugated anti-mouse CD8a (clone 53–6.7, Invitrogen) and PE-Cyanine 7-conjugated anti-mouse CD4 (clone GK1.5, eBioscience).

Cells were analyzed on a FACSCanto flow cytometer using BD FACSDiva software (BD Biosciences) and data analyzed using FlowJo v10 (FlowJo, LLC).

Immunofluorescence

Cells were seeded into 4-well chamber slides (Nugene) and treated accordingly based on experimental conditions. Following treatment at specified time points (24-hour post-irradiation), cells were fixed in 4% paraformaldehyde for 20 minutes are room temperature. Cells were then washed 3x with PBS stained with PBS containing DAPI. After DAPI staining, the well chamber was removed and coverslips were mounted in Vectashield Hard Set mounting media (Vector Labs). Images were captured using a Zeiss AxioImager 2 microscope using a 20x and 40x air objective and Zeiss ZEN Pro 2012 software. Images were prepared for publication using ImageJ (NIH) and adjusted only for brightness and contrast. Micronucleated cells were counted manually by identifying distinct staining of structures by DAPI outside of the main nucleus. Quantification of micronuclei was performed on at least 100 cells from each of three independent experiments. cGAS-positive micronuclei were counted by first identifying cells expressing the mCherry construct and similarly identifying mCherry and DAPI co-stained structures outside the main nucleus.

STING-Knockdown

The small-interfering RNAs (siRNAs) SMARTpool: ON-TARGETplus Mouse TMEM173 siRNA (L-055528–00-0005) and SMARTpool: ON-TARGETplus Human TMEM173 siRNA (L-024333–00-0005) were synthesized from Dharmacon (Lafayette, CO, USA) and were used to target TMEM173 (STING). As a negative control the ON-TARGETplus Non-Targeting Control Pool (D-001810–10-05, Dharmacon) was used.

MCF10A and B16F10 cells were seeded at a density of 2×10^5 cells per well in a six-well plate and transected with 60nM concentration of each siRNA utilizing Lipofectamine RNAiMAX Transfection Reagent (13778–150, Invitrogen) according to the manufacturer's instructions. Transfection was performed for 6 hours and the cells were used for evaluation 48 hours post-transfection. RT-qPCR was used to confirm the knockdown efficiency of the siRNAs.

RNA extraction, quantitative reverse transcription (RT) PCR

Total RNA was isolated from cells and tumors using the Qiagen RNeasy Mini kit (Qiagen #74106) at 24 hours post-irradiation as indicated. cDNA synthesis was performed using the High Capacity cDNA Reverse Transcription kit (Invitrogen). For each gene of interest, reactions were prepared in triplicate using 20ng of diluted cDNA and the appropriate Taqman gene expression master mix as per manufacturer's protocol (Mouse *CCL5*-Cat # Mm01302427_m1, Mouse *IFNB1*-Cat # Mm00439552_s1, Mouse *IFN-γ*-Cat # Mm01168134_m1, Mouse *GZMB*-Cat # Mm00442834_m1, Mouse *PRF1*-Cat # Mm00812512_m1, Mouse *GAPDH*-Cat # Mm99999915_g1, Human *CCL5*-Cat # Hs00982282_m1, Human *IFNB1*-Cat # Hs01077958_s1, Human *GAPDH*-Cat # Hs02786624_g1). Samples were run on the QuantStudio 6 Flex (Applied Biosystems by life technologies utilizing the QuantStudio™ Real-Time PCR software. Cycle threshold values

were determined for the genes of interest and by using the ΔΔCt method were normalized to GAPDH.

Immunoblotting

Cells were lysed in RIPA Extraction Buffer (89900, Thermo Fisher) with protease (1. complete Mini, EDTA free,11836170001, Roche, 2. Protease Inhibitor cocktail, P8340, Sigma) and phosphatase inhibitor cocktails (1. Halt™ Phosphatase Inhibitor cocktail, 1861277, Thermo Scientific, 2. Phosphatase Inhibitor cocktail 2 (P5726, Sigma) and 3 (P0044, Sigma)) following treatment with RT and/or AZD7762 as per the treatment group. Protein supernatant collection was performed at the indicated time points and quantified using the BCA Assay (Pierce). A total of 40μg of each protein lysate were loaded for separation by a 10% discontinuous SDS-Page gel. Transfer to 0.45μm PVDF membrane (IPVH00010, Merck Millipore) was performed using standard Western blotting methods. All different experimental condition lysates were loaded in the same gel and transferred in the same membrane. The membranes were blocked, for 1 hour at room temperature, in 5% (weight/volume) non-fat dry milk in TBS containing 0.05% Tween-20 followed by an overnight incubation at 4 °C with the phospho-STAT1 (Tyr701) (1:1000, #9167, Cell Signaling, RRID:AB_561284). Then, the membranes were hybridized with the appropriate secondary antibodies (1:2000, Goat pAb to Rb IgG (HRP, ab6721, Abcam) and developed in Amersham ECl western blotting detection reagents analysis system (RPN2209, GE Healthcare). Images of the blots were captured in ChemiDoc MP hi-end imaging system (Bio-Rad).

ELISA

5×10^4 B16F10 cells were seeded in a 24 well plate and incubated overnight to facilitate adherence. Cells were treated with 25nM AZD7762 (CHK1i) and 4Gy (RT) as appropriate, and the cell culture medium was collected 2 days post-irradiation. The VeriKine™ Mouse Interferon Beta ELISA kit (Cat# 42400, PBL Assay Science) was used according to the manufacturer's instructions.

In vivo Studies

8-week-old female C57BL/6 mice were obtained from Jackson Labs (RRID:IMSR_JAX:000664) and maintained under institutional animal husbandry and welfare protocols. All animal experiments were performed according to Institute of Animal Care and Use Committee (IACUC) protocols (Protocol # 805566) approved at the University of Pennsylvania. 2×10^5 B16-F10 cells mixed with an equal volume of Matrigel® Growth Factor Reduced (GFR) Basement Membrane Matrix (356231, Corning) were injected in the right flank (primary tumor) on Day 0, and then again in the left flank (abscopal tumor) on Day 2. Once palpable tumors had developed (Day 8), mice were re-sorted into cages in order to create an equal distribution of tumor volumes within each treatment group. AZD7762 was injected intraperitoneally on Day 9 at a concentration of 20mg/kg diluted in 0.9% sterile saline. The right flank (primary tumor) was irradiated with 17 Gy on Day 10 utilizing the Small Animal Radiation Research Platform (SARRP) with a 10 mm diameter circular collimator. 17 Gy was selected as a dose adequate to provide transient local tumor control without excess toxicity informed by prior studies (24) and adjusted based on prior

experience[24]. The scattered radiation dose contribution to the non-target contralateral flank tumor is estimated to be <0.3% of the total dose, or <0.05 Gy, based on prior film dosimetry verification performed on the SARRP apparatus. Tumor growth was monitored every two days using digital calipers to measure the perpendicular tumor diameters. Volume was calculated using the L x W^2 X 0.52 formula. Additional animals in the RT, AZD7762, and AZD7762+RT groups were sacrificed at Day 13 post-irradiation, and the primary and abscopal tumors were harvested and processed for flow cytometry cell sorting studies or snap frozen for gene expression studies (RT-qPCR). Mouse studies were not blinded given nature of differential treatments.

Statistical analyses

Student's unpaired, two-tailed t-test was used to test statistical significance in the micronuclei numbers and gene expression data. The Kaplan-Meier method was used to analyze differences in the tumor progression in the primary and abscopal tumors in the *in vivo* data to analyze tumor response. A threshold of 500 cc tumor volume was used to define progression, which was set based on the level of tumor volume achieved in directly irradiated tumors. Differences in *in vivo* tumor response were analyzed by employing the log-rank test to perform comparisons between treatment groups with all comparisons made to the untreated cohort.

Results

AZD7762 abrogates G2/M cell cycle arrest following RT

In order to confirm the ability of the Chk1/2 inhibitor, AZD7762, to promote cell cycle progression following radiation in our *in vitro* models, we first treated MCF10A breast epithelial cells and B16-F10 melanoma cells with AZD7762 and ionizing radiation, and assessed cell cycle distribution by flow cytometry. MCF10A cells received 16 Gy of ionizing radiation and B16-F10 cells received 4 Gy, with doses chosen to allow for subsequent survival and proliferation. Cells were fixed at 8 hours post-irradiation in order to capture cell-cycle arrest. For both MCF10A and B16-F10 cells, ionizing radiation resulted in significant G2/M block as indicated by an increase in the G2/M population by flow cytometry (Fig. 1). Treatment with AZD7762 alone did not cause a significant redistribution in the cell cycle as compared to untreated cells. Cells treated with AZD7762 (indicated by CHK1i in figures) prior to ionizing radiation (CHK1i + RT) exhibited a cell cycle profile similar to that of unirradiated cells indicating abrogation of the G2/M checkpoint allowing for cell cycle progression through mitosis (Fig. 1).

AZD7762+RT results in increased cGAS co-localized micronuclei formation

Given prior studies showing that inhibition of cell cycle progression prevents entry into mitosis and micronuclei formation[16], we tested our hypothesis that promoting mitotic progression after induction of DNA damage would result in increased micronuclei formation. Cells undergoing no treatment, AZD7762 treatment alone, or receiving 16 Gy of RT, all had ~5% micronucleated cells (5.0%, 5.1% and 5.3%, respectively), whereas MCF10A cells receiving the AZD7762+RT combination had 15.8% micronucleated cells, an approximate 3-fold increase and significantly more as compared to radiation alone (p

<0.001) (Fig. 2A). A similar effect was seen in B16-F10 melanoma cells, with 4.9% micronucleated cells in the untreated condition, 9.4% when receiving AZD7762 alone, and 5.3% with 4 Gy RT. The combination of AZD7762+RT again resulted in a marked increase of micronucleated cells with 36.6% of cells developing micronuclei, which was significantly more compared to the untreated and single treatment conditions (all p <0.001) (Fig. 2B). The same trend of a significant increase in micronucleated cells with the AZD7762+RT combination was observed in other cell lines as well (H460, H1299) (Supplementary Fig. 1).

We also sought to determine if the increased micronuclei generated by the AZD7762+RT combination maintained the ability to co-localize with cGAS as a link to subsequent downstream immune gene signaling, based on previous literature[16]. MCF10A cells were stably infected with lentivirus containing a mCherry-cGAS plasmid, resulting in approximately 15–20% expression of mCherry-cGAS. We observed a diffuse cytoplasmic signal for cGAS in unirradiated mCherry-cGAS-expressing cells that do not form micronuclei (Fig. 3A, C and E). In contrast, when micronuclei were present, we observed a localized hyperintense mCherry-cGAS signal co-localizing to the micronucleus, as seen in representative cells treated with AZD7762+RT (Fig. 3B, D and F). This staining pattern was seen across all treatment conditions, and in all cases where a cell simultaneously expressed mCherry-cGAS and developed micronuclei, there was universal cGAS-micronuclei co-localization. The percentage of cGAS-co-localized micronucleated cells for each treatment condition mirrored that of the overall micronuclei population (Fig. 3G).

AZD7762+RT treatment results in increased immune gene signaling

We next sought to determine the impact on immune signaling in the context of increased micronuclei formation with AZD7762+RT treatment. We analyzed the relative gene expression of the Type-I interferon regulated genes *IFN-β* and *CCL5,* which were chosen due to their role as downstream effectors in the cGAS-STING pathway via the IRF3 transcription factor[8, 13, 17]. In MCF10A cells, when compared to the untreated condition, RT alone did not result in a large change in mRNA levels of *IFN-β* or *CCL5* at the 24-hour post-treatment time-point (1.3-fold increase for both genes, p = 0.4). When AZD7762+RT was delivered however, there was a significant 5.5-fold increase (p = .02) in *IFN-β* mRNA expression and a 21-fold increase (p <.001) in *CCL5* mRNA expression (Fig. 4A and B). Similarly, AD7762+RT resulted in significant upregulation of both these genes over that seen with RT alone (p < 0.001).

In B16-F10 cells, RT alone did not result in an increase in *IFN-β* expression (0.9 fold, p = 0.72) but did result in increased *CCL5* expression (2.3-fold, p = .008). AZD7762+RT was associated with a 1.8-fold increase in *IFN-β* mRNA (p = .03), and an even greater increase in *CCL5* expression, 4.3-fold (p = <.001) (Fig. 4C and D). AZD7762+RT also resulted in a significant increase in expression of both *IFN-β* and *CCL5* as compared to RT alone (p = 0.02, p = 0.001, respectively). *IFN-β* secreted protein in B16-F10 cell culture was quantified by ELISA and mirrored the mRNA expression pattern, with significantly increased protein levels in the AZD7762+RT as compared to RT alone (19.8 pg/nL vs. 11.8 pg/nL p <0.001) (Fig. 5).

We proceeded to assess downstream signaling events driven by the cGAS-STING pathway by measuring STAT1 phosphorylation. Prior studies showed that upregulated IFN-β signaling following activation of the cGAS-STING pathway is capable of driving phosphorylation of STAT1 [18, 19]. As with the gene expression data, we found that STAT1 phosphorylation also increased the most profoundly after combination AZD7762+RT treatment in both MCF10A and B16-F10 cells at multiple time points (Fig. 4E and F). The AZD7762+RT combination showed pSTAT1 levels on par or greater than that driven by diallyl disulfide, which was used as a positive control for pSTAT1 [21]. In contrast, treatment with AZD7762 or radiation alone in either cell line did not result in noticeable increases in pSTAT1 levels.

To confirm that the observed activation of the immune response was mediated through the cGAS-STING pathway, MCF10A cells were transfected with siRNA pools against *STING* or control (non-targeting) siRNA and exposed to the same experimental conditions. In MCF10A cells transfected with control siRNA and exposed to AZD7762+RT, we observed a dramatic increase in *CCL5* and *IFN-β* mRNA as compared to cells exposed to AZD7762 or RT alone. However, when STING expression was downregulated using siRNA, the expression of *CCL5* and *IFN-β* mRNA after AZD7762+RT exposure was significantly lower as compared to control siRNA-transfected cells (*CCL5:* 242.8 vs. 99.9 fold, $p < 0.001$; *IFN-β:* 39.6 vs. 9.7 fold, $p < 0.001$) (Fig. 4G and H).

In vivo mouse study results

In vivo testing was also performed using C57BL6 mice implanted with B16-F10 melanoma cells in the right flank to create the primary tumor and two days later in the left flank to create the abscopal tumor. Within the primary tumor, the groups receiving radiation (RT) with 17 Gy, or AZD7762+RT all uniformly had controlled tumors at the treated site (both $p < 0.001$). A higher RT dose of 17 Gy was used in these *in vivo* experiments as opposed to 4 Gy in the *in vitro* experiments given inadequate duration of tumor control with smaller radiation doses from prior experience and informed by earlier clinical studies[24]. Mice treated with AZD7762 alone showed a trend toward improved tumor control, but no significant change in the overall rate and time course of tumor progression when compared to untreated mice ($p = 0.17$) (Fig. 6A).

At the abscopal site, which was not directly irradiated, neither radiation nor AZD7762 alone resulted in significantly improved tumor control compared to untreated mice ($p = 0.13$, $p = 0.09$ respectively). However, the combination of AZD7762+RT showed significantly improved tumor control at the abscopal site ($p < 0.001$) (Fig. 6B, Supplementary Fig. 2).

The average tumor volume for each group within the primary and abscopal sites mirrors these findings. Within the primary tumor, the mean tumor volume at Day 10 post treatment was 160 +/− 21 cc in the RT group and 108 +/− 24cc in the AZD7762+RT group. This is in contrast to the much larger tumor volume observed in the two unirradiated groups where the mean tumor volume was 1869 +/− 234 cc in the untreated mice and 1493 +/− 259 cc in the mice receiving AZD7762 alone (Fig. 7A). Within the abscopal site, the AZD7762+RT treated mice exhibited the lowest mean tumor volume at Day 10 at 638 +/− 184 cc as

compared to 1152 +/− 169 cc in the untreated group, 1179 +/− 129 cc in the RT alone group and 905 +/− 129 cc in the AZD7762 alone group (Fig. 7B).

In vivo Immune Activation

In order to directly assess immune cell recruitment and activation given the putative immune-promoting effects of the AZD7762+RT combination, we analyzed the CD8 T-cell population within the primary and abscopal tumors of the treated mice. Animals were sacrificed 13 days post-radiation, and the primary and unirradiated (abscopal) tumors were harvested and analyzed by FACS to quantify the CD8+ T-cell population. Within the directly radiated primary tumors, there was a significant increase in CD8+ cells with both RT and AZD7762+RT as compared to mice treated with AZD7762. The AZD7762+RT treated tumors additionally had significantly more CD8+ cells as compared to RT alone (80% vs. 70%, p = 0.048). Within the unirradiated abscopal tumors, mice treated with RT or AZD7762 alone did not significantly differ in the CD8+ population. However, the AZD7762+RT treated mice had a significantly higher CD8+ population in the abscopal tumor as compared to either the RT (33% vs. 10%, p = 0.002) or AZD7762 (33% vs. 15%, p = 0.005) (Fig. 8A and B).

Similarly, we examined comparative gene expression of immune activation markers in the primary and abscopal tumor sites. Within the primary irradiated tumor, increased expression of the markers *IFN-γ* (12-fold increase, p = 0.06), and *GZMB* (12.5-fold increase, p = 0.02) was observed with AZD7762+RT vs. RT alone (Fig. 8C and D). The abscopal unirradiated tumor had an even more profound response, with significantly increased expression of *IFN-γ* (33-fold increase, p = 0.04), and *GZMB* (50-fold increase, p = 0.03) with AZD7762+RT vs. RT alone (Fig. 8E and F).

Discussion

In this work, we utilized the Chk1/2i inhibitor, AZD7762 in conjunction with ionizing radiation to provide proof of principle that pharmacologically forcing cell cycle progression following genotoxic stress is able to cause a resultant increase in the formation of micronuclei. This builds upon models shown in prior work indicating that cell cycle progression through mitosis coupled with DNA damage are the necessary factors for micronuclei formation[11, 16], and that cell cycle checkpoint kinase inhibition can drive mitotic catastrophe, inflammatory signaling, and cell-intrinsic and extrinsic anti-tumor activity [25, 31, 34]. Furthermore, we show that the combination treatment leads to increased expression of IFN-β mRNA and protein *in vitro* and an effect on an abscopal (unirradiated) tumor *in vivo* with increased expression of genes involved in immune activation and increased CD8+ T-cell infiltration, consistent with an increased systemic immune response.

Cell cycle checkpoint inhibitors, including AZD7762 itself [27, 43], have previously been explored as radiosensitizers and have demonstrated the ability to synergistically work with ionizing radiation to improve tumor control through abrogation of cell cycle checkpoints and inhibition of DNA repair. To this point, there is an ongoing clinical trial using prexasertib[44], a Chk1/2 inhibitor with radiation and cetuximab in locally advanced head and neck squamous cell carcinoma (NCT02555644). Our work takes an alternative mechanistic

approach to exploring the potential benefits of Chk1/2 inhibitors by focusing on micronuclei induction, and more importantly, their link with immune gene activation.

Prior studies suggest that micronuclei can be expected to increase when radiation is combined with other inhibitors of cell cycle checkpoint factors including ATR1 and Chk1 alone[9]. Given the increasing understanding of the importance of the immune system on tumor control, we focused on the interplay between the ability of ionizing radiation and cell cycle checkpoint inhibitor combinations to form increased micronuclei and the ability of micronuclei to activate the cGAS-STING pathway [6, 8, 10, 13, 17, 23, 33, 40, 41]. In this study, we found that the increase in micronuclei created by combining AZD7762+RT is able to drive downstream immune gene activation through co-localization with cGAS and increased cGAS-STING signaling. Furthermore, the associated increase in Type-I interferon gene expression seen with increased micronuclei formation was decreased upon knockdown of STING, emphasizing the role of the cGAS-STING pathway in the process. In the *in vivo* setting, the AZD7762+RT combination was also able to drive increased immune cell recruitment in implanted mouse tumors.

The ability of cell cycle checkpoint inhibitors to act as direct radiosensitizers and improve control of irradiated tumors has been demonstrated in the past[27], but given the potential immune-stimulating effects of AZD7762, we also focused on its ability to work in conjunction with radiation to drive abscopal tumor responses through an immune-mediated mechanism. Immune checkpoint inhibitors targeting genes such as *PD-1* and *PDL-1* have revolutionized clinical oncology, and both *in vivo* mouse studies, and clinical experiences in humans have demonstrated their ability to lead to abscopal tumor regression in concert with ionizing radiation[28, 36]. However, given that success with the use of immune checkpoint inhibitors is not universal, the need to develop additional agents remains. Our data here, using a series of experiments specifically designed to promote immunogenic events, demonstrates significant enhancements in abscopal tumor control with AZD7762+RT over other treatments. By extension, this suggests that other cell cycle checkpoint inhibitors besides AZD7762 may have the capability of causing similar tumor regression. This lends promise to the continued exploration of this class of agents to induce not only local, but also systemic responses.

Along these lines, there is potential value in exploring agents that affect targets besides Chk1/2i as they may show variable efficacy. There are data that suggest that ATR inhibitors are more potent inducers of micronuclei than Chk1 inhibitors [9] and may potentiate CD8+ T cell antitumor activity with radiation[37]. Targeted inhibition of Wee1 has also been shown to promote mitotic entry causing increased micronuclei formation [1, 26] and separate studies have reported that Wee1 inhibition relieves cancer cell system to lysis by antigen-specific T cells and natural killer cells [15]. There is also recent clinical data showing safety and efficacy of the Wee1 inhibitor adavosertib in combination with ionizing radiation [7]. While our study utilized AZD7762, there is certainly merit in exploring other therapeutic combinations, including other agents targeting Chk1 and Chk2[14].

Alternative dose fractionation schemes may also further inform our work and provide additional opportunities to alter the level of immune activation. The optimal radiation

activation scheme is an active area of debate and in our work, we utilized a single large dose of radiation *in vivo,* in keeping with our previous clinical experience[24]. This is in contrast to more clinically common conventionally fractionated treatment regimens, with multiple smaller doses. The ultimate clinical application of treatment regimens combining ionizing radiation and cell cycle checkpoint inhibitors will require a balance of convenience, safety, and efficacy of immune activation in order to achieve favorable responses.

Another prospective avenue to further improve the potential for abscopal tumor regression would be to combine immune checkpoint inhibition in addition to radiation and cell cycle checkpoint inhibition. There is precedent for an increased tumor response with the use of dual checkpoint immune blockade with ionizing radiation[36], where increased rates of complete tumor response were seen with triple combination therapy over double combination therapy. Utilizing the same biologic principles, the addition of immune checkpoint blockade (e.g. anti PDL-1, anti CTLA-4 agents) to our AZD7762+RT combination could be even more efficacious and represents a potential avenue for future exploration.

Conclusions

Overall, our findings show that cell cycle progression through mitosis with ionizing radiation is a viable means by which to increase micronuclei formation and cause immune activation resulting in abscopal tumor responses. There is potential for the expanded use of this class of agents which are currently being tested in the clinic, beyond direct radiation, with many potential avenues for further investigation in order to improve systemic tumor response.

Supplementary Material

Refer to Web version on PubMed Central for supplementary material.

Acknowledgments

This study was supported by NIH/NCI grant (1R01CA182747-01A1 (PI: Maity, Koumenis) and the University of Pennsylvania Radiation Oncology Resident Research Award (to H. Chao). The authors thank Roger Greenberg group for contribution of cGAS constructs.

References

1. Aarts M, Sharpe R, Garcia-Murillas I, Gevensleben H, Hurd MS, Shumway SD et al. Forced mitotic entry of S-phase cells as a therapeutic strategy induced by inhibition of WEE1. Cancer Discov 2012; 2: 524–539. [PubMed: 22628408]
2. al-Khodairy F, Fotou E, Sheldrick KS, Griffiths DJ, Lehmann AR, Carr AM. Identification and characterization of new elements involved in checkpoint and feedback controls in fission yeast. Mol Biol Cell 1994; 5: 147–160. [PubMed: 8019001]
3. Borghaei H, Paz-Ares L, Horn L, Spigel DR, Steins M, Ready NE et al. Nivolumab versus Docetaxel in Advanced Nonsquamous Non-Small-Cell Lung Cancer. N Engl J Med 2015; 373: 1627–1639. [PubMed: 26412456]
4. Brahmer J, Reckamp KL, Baas P, Crino L, Eberhardt WE, Poddubskaya E et al. Nivolumab versus Docetaxel in Advanced Squamous-Cell Non-Small-Cell Lung Cancer. N Engl J Med 2015; 373: 123–135. [PubMed: 26028407]

5. Canman CE, Lim DS, Cimprich KA, Taya Y, Tamai K, Sakaguchi K et al. Activation of the ATM kinase by ionizing radiation and phosphorylation of p53. Science 1998; 281: 1677–1679. [PubMed: 9733515]
6. Chen Q, Sun L, Chen ZJ. Regulation and function of the cGAS-STING pathway of cytosolic DNA sensing. Nat Immunol 2016; 17: 1142–1149. [PubMed: 27648547]
7. Cuneo KC, Morgan MA, Sahai V, Schipper MJ, Parsels LA, Parsels JD et al. Dose Escalation Trial of the Wee1 Inhibitor Adavosertib (AZD1775) in Combination With Gemcitabine and Radiation for Patients With Locally Advanced Pancreatic Cancer. J Clin Oncol 2019: JCO1900730.
8. Deng L, Liang H, Xu M, Yang X, Burnette B, Arina A et al. STING-Dependent Cytosolic DNA Sensing Promotes Radiation-Induced Type I Interferon-Dependent Antitumor Immunity in Immunogenic Tumors. Immunity 2014; 41: 843–852. [PubMed: 25517616]
9. Dillon MT, Barker HE, Pedersen M, Hafsi H, Bhide SA, Newbold KL et al. Radiosensitization by the ATR Inhibitor AZD6738 through Generation of Acentric Micronuclei. Mol Cancer Ther 2017; 16: 25–34. [PubMed: 28062704]
10. Diner EJ, Burdette DL, Wilson SC, Monroe KM, Kellenberger CA, Hyodo M et al. The innate immune DNA sensor cGAS produces a noncanonical cyclic dinucleotide that activates human STING. Cell Rep 2013; 3: 1355–1361. [PubMed: 23707065]
11. Dou Z, Ghosh K, Vizioli MG, Zhu J, Sen P, Wangensteen KJ et al. Cytoplasmic chromatin triggers inflammation in senescence and cancer. Nature 2017; 550: 402–406. [PubMed: 28976970]
12. Gandhi L, Rodriguez-Abreu D, Gadgeel S, Esteban E, Felip E, De Angelis F et al. Pembrolizumab plus Chemotherapy in Metastatic Non-Small-Cell Lung Cancer. N Engl J Med 2018; 378: 2078–2092. [PubMed: 29658856]
13. Grandvaux N, Servant MJ, tenOever B, Sen GC, Balachandran S, Barber GN et al. Transcriptional profiling of interferon regulatory factor 3 target genes: direct involvement in the regulation of interferon-stimulated genes. J Virol 2002; 76: 5532–5539. [PubMed: 11991981]
14. Guzi TJ, Paruch K, Dwyer MP, Labroli M, Shanahan F, Davis N et al. Targeting the replication checkpoint using SCH 900776, a potent and functionally selective CHK1 inhibitor identified via high content screening. Mol Cancer Ther 2011; 10: 591–602. [PubMed: 21321066]
15. Hamilton DH, Huang B, Fernando RI, Tsang KY, Palena C. WEE1 inhibition alleviates resistance to immune attack of tumor cells undergoing epithelial-mesenchymal transition. Cancer Res 2014; 74: 2510–2519. [PubMed: 24626094]
16. Harding SM, Benci JL, Irianto J, Discher DE, Minn AJ, Greenberg RA. Mitotic progression following DNA damage enables pattern recognition within micronuclei. Nature 2017; 548: 466–470. [PubMed: 28759889]
17. Hartlova A, Erttmann SF, Raffi FA, Schmalz AM, Resch U, Anugula S et al. DNA damage primes the type I interferon system via the cytosolic DNA sensor STING to promote anti-microbial innate immunity. Immunity 2015; 42: 332–343. [PubMed: 25692705]
18. Ishikawa H, Ma Z, Barber GN. STING regulates intracellular DNA-mediated, type I interferon-dependent innate immunity. Nature 2009; 461: 788–792. [PubMed: 19776740]
19. Karpova AY, Trost M, Murray JM, Cantley LC, Howley PM. Interferon regulatory factor-3 is an in vivo target of DNA-PK. Proc Natl Acad Sci U S A 2002; 99: 2818–2823. [PubMed: 11867762]
20. Kastan MB, Onyekwere O, Sidransky D, Vogelstein B, Craig RW. Participation of p53 protein in the cellular response to DNA damage. Cancer Res 1991; 51: 6304–6311. [PubMed: 1933891]
21. Lu HF, Yang JS, Lin YT, Tan TW, Ip SW, Li YC et al. Diallyl disulfide induced signal transducer and activator of transcription 1 expression in human colon cancer colo 205 cells using differential display RT-PCR. Cancer Genomics Proteomics 2007; 4: 93–97. [PubMed: 17804871]
22. Ma CX, Janetka JW, Piwnica-Worms H. Death by releasing the breaks: CHK1 inhibitors as cancer therapeutics. Trends Mol Med 2011; 17: 88–96. [PubMed: 21087899]
23. Mackenzie KJ, Carroll P, Martin CA, Murina O, Fluteau A, Simpson DJ et al. cGAS surveillance of micronuclei links genome instability to innate immunity. Nature 2017; 548: 461–465. [PubMed: 28738408]
24. Maity A, Mick R, Huang AC, George SM, Farwell MD, Lukens JN et al. A phase I trial of pembrolizumab with hypofractionated radiotherapy in patients with metastatic solid tumours. Br J Cancer 2018; 119: 1200–1207. [PubMed: 30318516]

25. Melms JC, Vallabhaneni S, Mills CE, Yapp C, Chen JY, Morelli E et al. Inhibition of Haspin Kinase Promotes Cell-Intrinsic and Extrinsic Antitumor Activity. Cancer Res 2019.
26. Moran DM, Gawlak G, Jayaprakash MS, Mayar S, Maki CG. Geldanamycin promotes premature mitotic entry and micronucleation in irradiated p53/p21 deficient colon carcinoma cells. Oncogene 2008; 27: 5567–5577. [PubMed: 18504430]
27. Morgan MA, Parsels LA, Zhao L, Parsels JD, Davis MA, Hassan MC et al. Mechanism of radiosensitization by the Chk1/2 inhibitor AZD7762 involves abrogation of the G2 checkpoint and inhibition of homologous recombinational DNA repair. Cancer Res 2010; 70: 4972–4981. [PubMed: 20501833]
28. Postow MA, Callahan MK, Barker CA, Yamada Y, Yuan J, Kitano S et al. Immunologic correlates of the abscopal effect in a patient with melanoma. N Engl J Med 2012; 366: 925–931. [PubMed: 22397654]
29. Reck M, Rodriguez-Abreu D, Robinson AG, Hui R, Csoszi T, Fulop A et al. Pembrolizumab versus Chemotherapy for PD-L1-Positive Non-Small-Cell Lung Cancer. N Engl J Med 2016; 375: 1823–1833. [PubMed: 27718847]
30. Reck M Pembrolizumab as first-line therapy for metastatic non-small-cell lung cancer. Immunotherapy 2018; 10: 93–105. [PubMed: 29145737]
31. Schoonen PM, Kok YP, Wierenga E, Bakker B, Foijer F, Spierings DCJ et al. Premature mitotic entry induced by ATR inhibition potentiates olaparib inhibition-mediated genomic instability, inflammatory signaling, and cytotoxicity in BRCA2-deficient cancer cells. Mol Oncol 2019; 13: 2422–2440. [PubMed: 31529615]
32. Shaverdian N, Lisberg AE, Bornazyan K, Veruttipong D, Goldman JW, Formenti SC et al. Previous radiotherapy and the clinical activity and toxicity of pembrolizumab in the treatment of non-small-cell lung cancer: a secondary analysis of the KEYNOTE-001 phase 1 trial. Lancet Oncol 2017; 18: 895–903. [PubMed: 28551359]
33. Sun L, Wu J, Du F, Chen X, Chen ZJ. Cyclic GMP-AMP synthase is a cytosolic DNA sensor that activates the type I interferon pathway. Science 2013; 339: 786–791. [PubMed: 23258413]
34. Tao Y, Leteur C, Calderaro J, Girdler F, Zhang P, Frascogna V et al. The aurora B kinase inhibitor AZD1152 sensitizes cancer cells to fractionated irradiation and induces mitotic catastrophe. Cell Cycle 2009; 8: 3172–3181. [PubMed: 19755861]
35. Thomas C, Rajapaksa G, Nikolos F, Hao R, Katchy A, McCollum CW et al. ERbeta1 represses basal breast cancer epithelial to mesenchymal transition by destabilizing EGFR. Breast Cancer Res 2012; 14: R148. [PubMed: 23158001]
36. Twyman-Saint Victor C, Rech AJ, Maity A, Rengan R, Pauken KE, Stelekati E et al. Radiation and dual checkpoint blockade activate non-redundant immune mechanisms in cancer. Nature 2015; 520: 373–377. [PubMed: 25754329]
37. Vendetti FP, Karukonda P, Clump DA, Teo T, Lalonde R, Nugent K et al. ATR kinase inhibitor AZD6738 potentiates CD8+ T cell-dependent antitumor activity following radiation. J Clin Invest 2018; 128: 3926–3940. [PubMed: 29952768]
38. Walworth N, Davey S, Beach D. Fission yeast chk1 protein kinase links the rad checkpoint pathway to cdc2. Nature 1993; 363: 368–371. [PubMed: 8497322]
39. Walworth NC, Bernards R. rad-dependent response of the chk1-encoded protein kinase at the DNA damage checkpoint. Science 1996; 271: 353–356. [PubMed: 8553071]
40. Woo SR, Fuertes MB, Corrales L, Spranger S, Furdyna MJ, Leung MY et al. STING-dependent cytosolic DNA sensing mediates innate immune recognition of immunogenic tumors. Immunity 2014; 41: 830–842. [PubMed: 25517615]
41. Woo SR, Corrales L, Gajewski TF. The STING pathway and the T cell-inflamed tumor microenvironment. Trends Immunol 2015; 36: 250–256. [PubMed: 25758021]
42. Xu B, Kim S, Kastan MB. Involvement of Brca1 in S-phase and G(2)-phase checkpoints after ionizing irradiation. Mol Cell Biol 2001; 21: 3445–3450. [PubMed: 11313470]
43. Zabludoff SD, Deng C, Grondine MR, Sheehy AM, Ashwell S, Caleb BL et al. AZD7762, a novel checkpoint kinase inhibitor, drives checkpoint abrogation and potentiates DNA-targeted therapies. Mol Cancer Ther 2008; 7: 2955–2966. [PubMed: 18790776]

44. Zeng L, Beggs RR, Cooper TS, Weaver AN, Yang ES. Combining Chk1/2 Inhibition with Cetuximab and Radiation Enhances In Vitro and In Vivo Cytotoxicity in Head and Neck Squamous Cell Carcinoma. Mol Cancer Ther 2017; 16: 591–600. [PubMed: 28138028]

45. Zhao H, Watkins JL, Piwnica-Worms H. Disruption of the checkpoint kinase 1/cell division cycle 25A pathway abrogates ionizing radiation-induced S and G2 checkpoints. Proc Natl Acad Sci U S A 2002; 99: 14795–14800. [PubMed: 12399544]

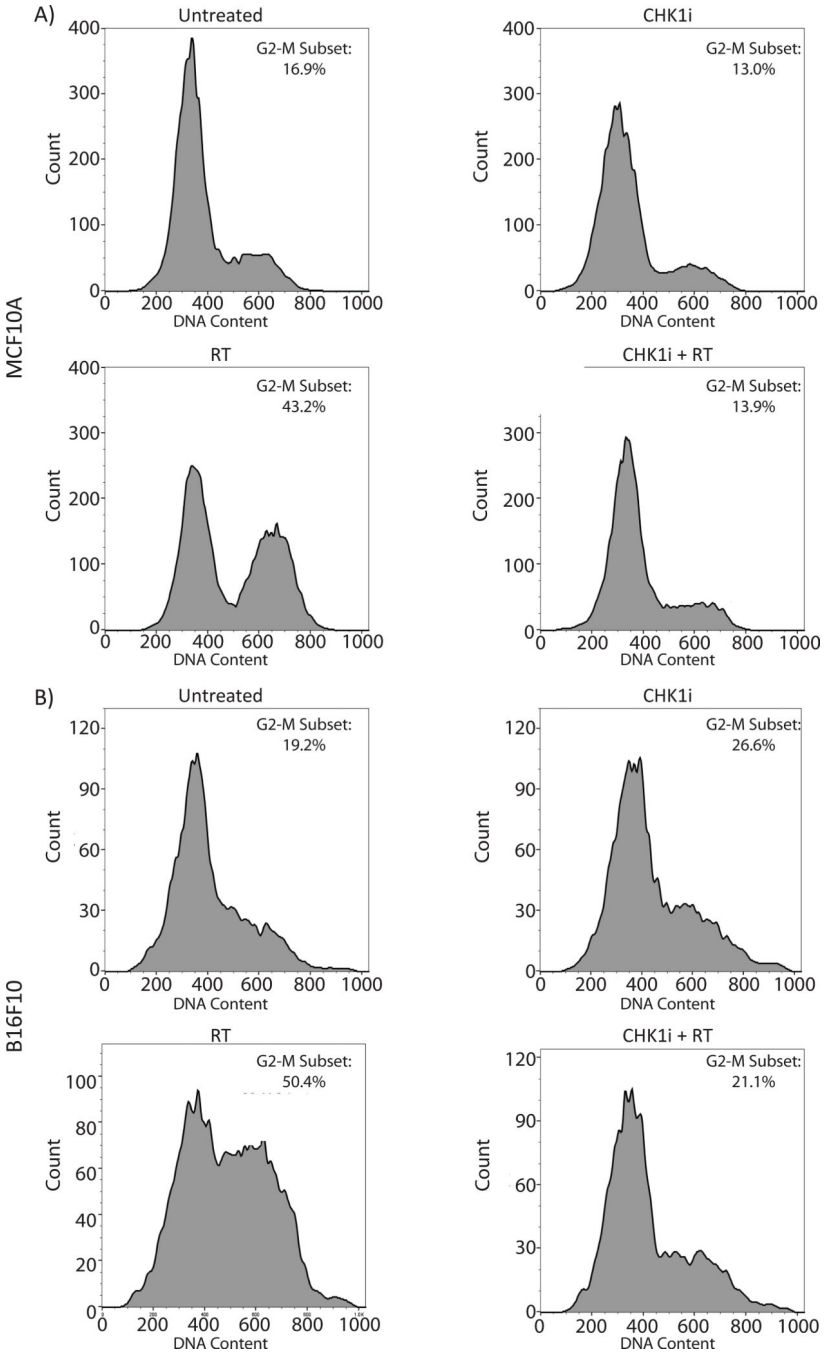

Figure 1: AZD7762 treatment abrogates RT induced G2/M Checkpoint

Flow cytometry analysis showing the cell cycle distribution by DNA content of A) MCF10A and B) B16-F10 cells by treatment status. Each cell lines had one of four treatment conditions: Untreated, or treated with the CHK1 inhibitor AZD7762, Radiation (RT), or CHK1i+RT. AZD7762 was added 1 hour prior to RT. MCF10A cells underwent 16 Gy of RT and B16-F10 underwent 4 Gy of RT. Cell fixation was performed at 8 hours following radiation for cell cycle analysis. The G2/M population is highlighted within each panel.

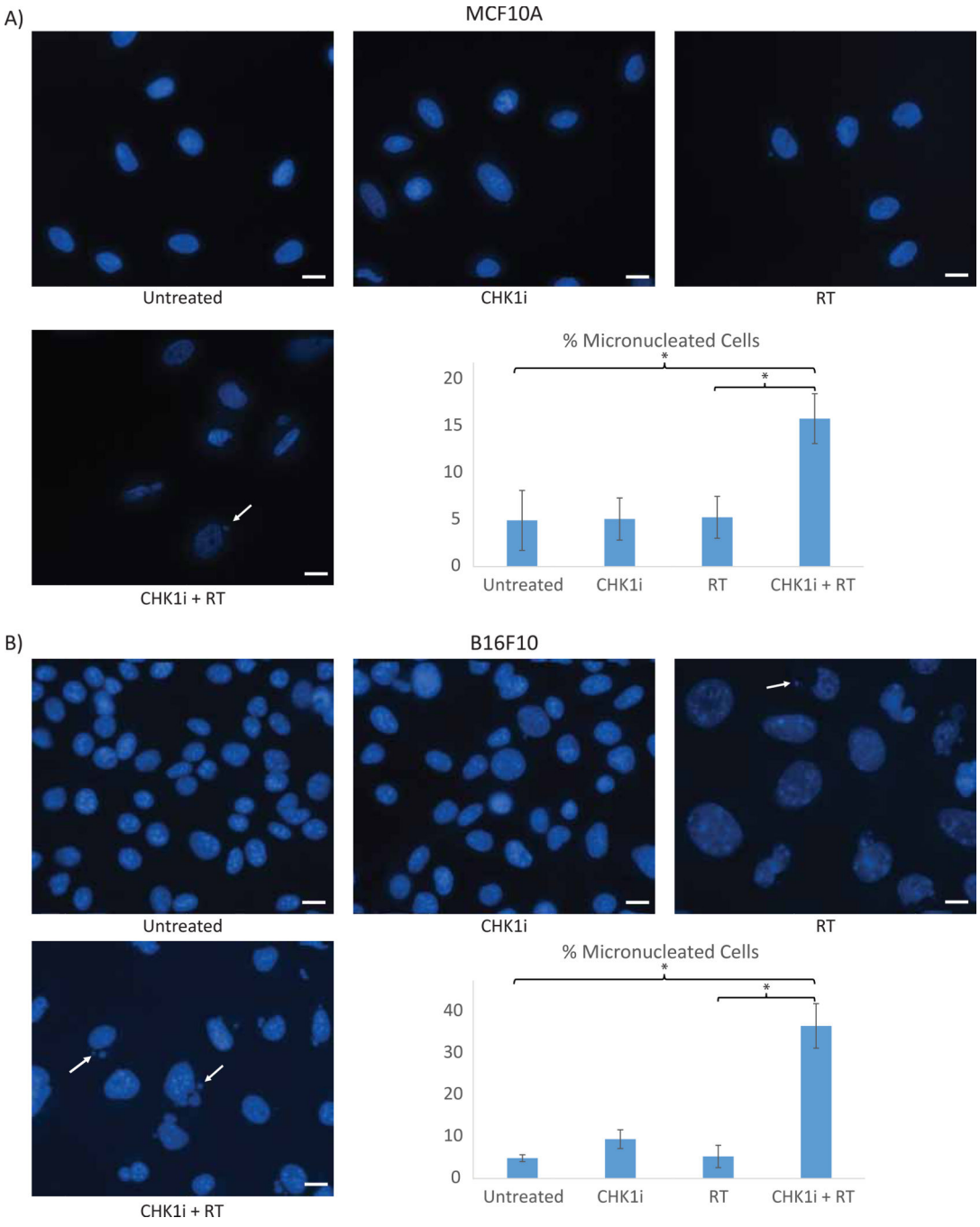

Figure 2: AZD7762+RT combination treatment increases micronuclei formation

Representative images of A) MCF10A and B) B16-F10 cells by treatment condition with quantitation of the percentage of micronucleated cells for each group at 24 hours following radiation (Untreated, CHK1i (AZD7762), RT, CHK1i (AZD7762)+RT). A) MCF10A cells underwent 16 Gy of RT and B) B16-F10 underwent 4 Gy of RT. Scale bar represents 10μM

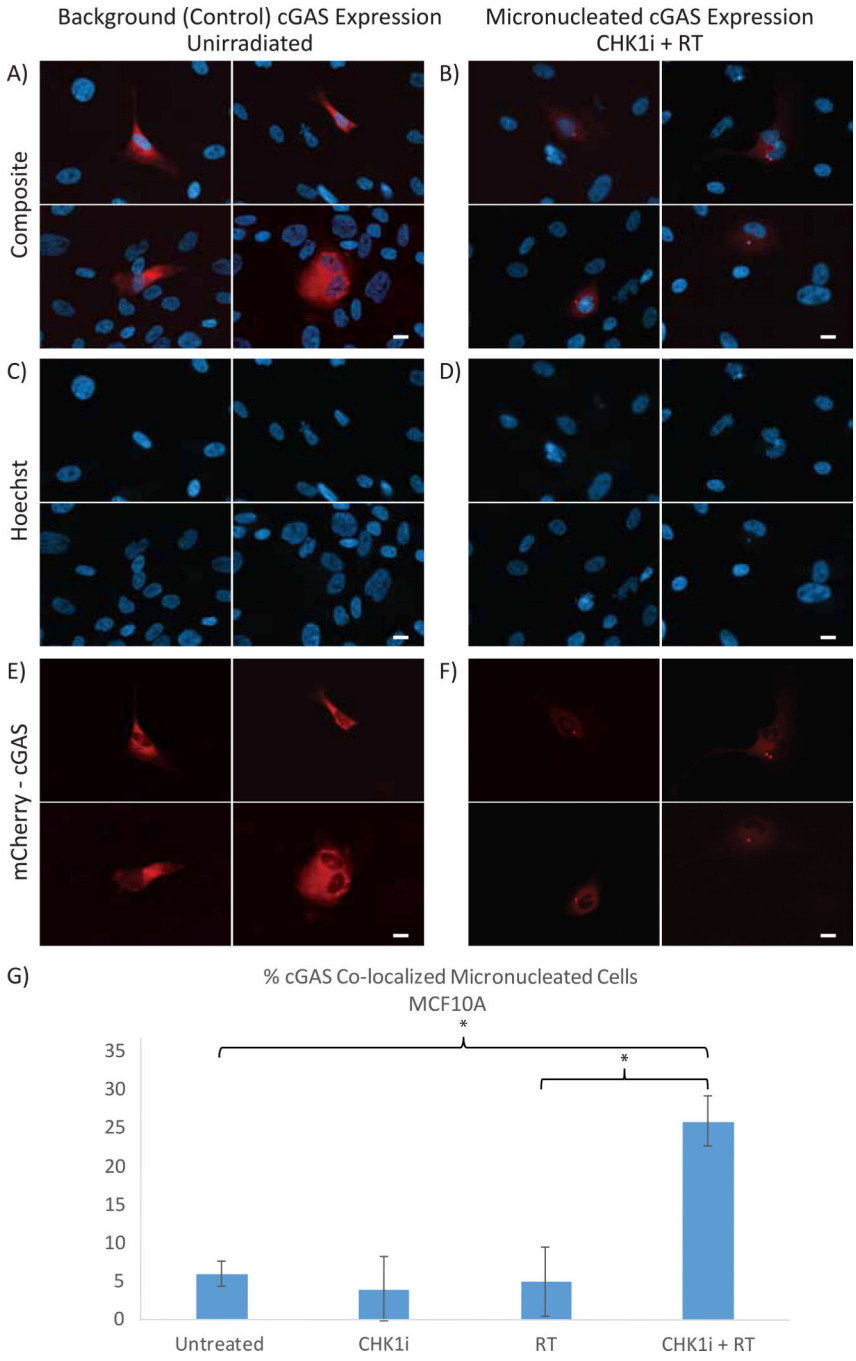

Figure 3: cGAS co-localizes with induced micronuclei

MCF10A cells expressing the mCherry-tagged cGAS construct (~15–20% of all cells) are shown within a background of non-stably transfected MCF10A cells. A,C,E) Representative images of MCF10A cells treated with CHK1i (AZD7762)+RT which express the mCherry-tagged cGAS construct in the absence of micronuclei in the Composite (A), Hoechst (C), and mCherry (E) channels. B,D,F) Representative images of MCF10A cells treated with CHK1i (AZD7762)+RT expressing the mCherry-cGAS construct in the presence of micronuclei formation in the Composite (B), Hoechst (E), and mCherry (F) channels. G)

The percentage of cGAS co-localized micronuclei with each treatment condition. All cells were analyzed at 24 hours following radiation. Scale bar represents 10μM

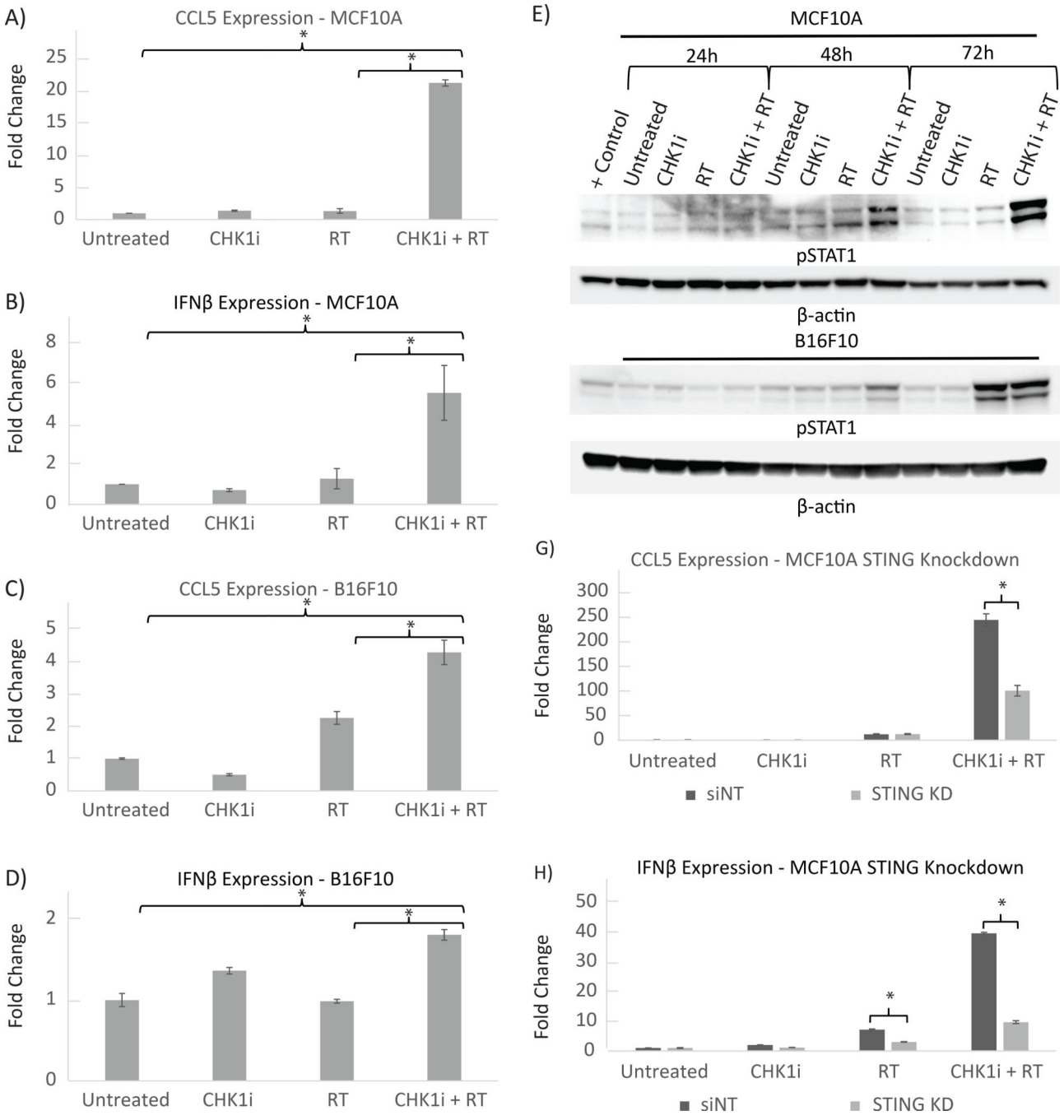

Figure 4: AZD7762+RT combination increases Type I interferon regulated gene and protein expression and is mediated through the *STING* pathway

A,B) Relative mRNA levels of MCF10A cells by treatment condition at 24 hours post-irradiation with each treatment group normalized to untreated cells is shown for A) *IFN-β* and B) *CCL5.* MCF10A cells received 16 Gy of ionizing radiation and CHK1i (AZD7762) was added to media 1 hour prior to RT. Values represent the mean ±S.D. of three experiments; *, $P \leq 0.05$.

C,D) Relative mRNA levels of B16-F10 cells by treatment condition at 24 hours post-irradiation with each treatment group normalized to untreated cells is shown for C) *IFN-β*

and D) *CCL5.* B16F10 cells received 4 Gy of ionizing radiation and CHK1i (AZD7762) was added to media 1 hour prior to RT. Values represent the mean ±S.D. of three experiments; *, $P \leq 0.05$.

E, F) Protein levels of phosphorylated STAT1 with Beta-Actin loading control is shown for E) MCF10A and F) B16-F10 cells at the 24, 48 and 72 hour time points as indicated. MCF10A cells underwent 16 Gy of RT and B16-F10 underwent 4 Gy of RT.

G, H) Relative mRNA levels of MCF10A cells with siRNA knockdown against non-template target *STING* for G) *IFN-β* and H) *CCL5.* MCF10A cells received 16 Gy of ionizing radiation and CHK1i (AZD7762) was added to media 1 hour prior to RT. Each treatment group is normalized to the untreated condition for the MCF10A non-template control Values represent the mean ±S.D. of three experiments; *, $P \leq 0.05$.

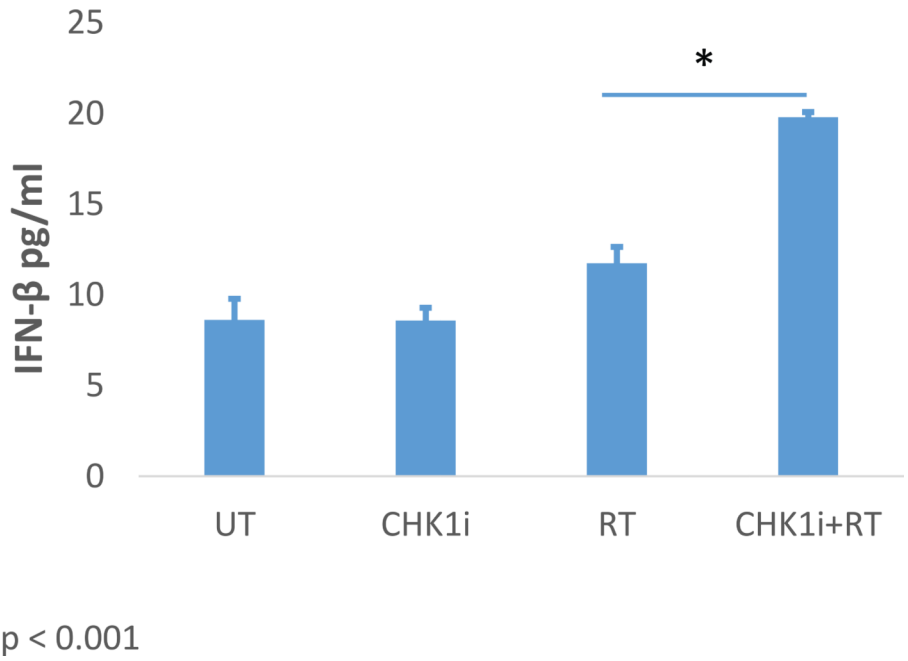

Figure 5: Secreted IFN-β Protein Expression by ELISA in B16F10 Tumor Cells

Protein expression levels of secreted IFN-β was assessed by ELISA in B16F10 cells by treatment condition at 48 hours post-irradiation. B16F10 cells received 4 Gy of ionizing radiation and CHK1i (AZD7762) was added to media 1 hour prior to RT. Values represent the mean ±S.D. of three experiments.

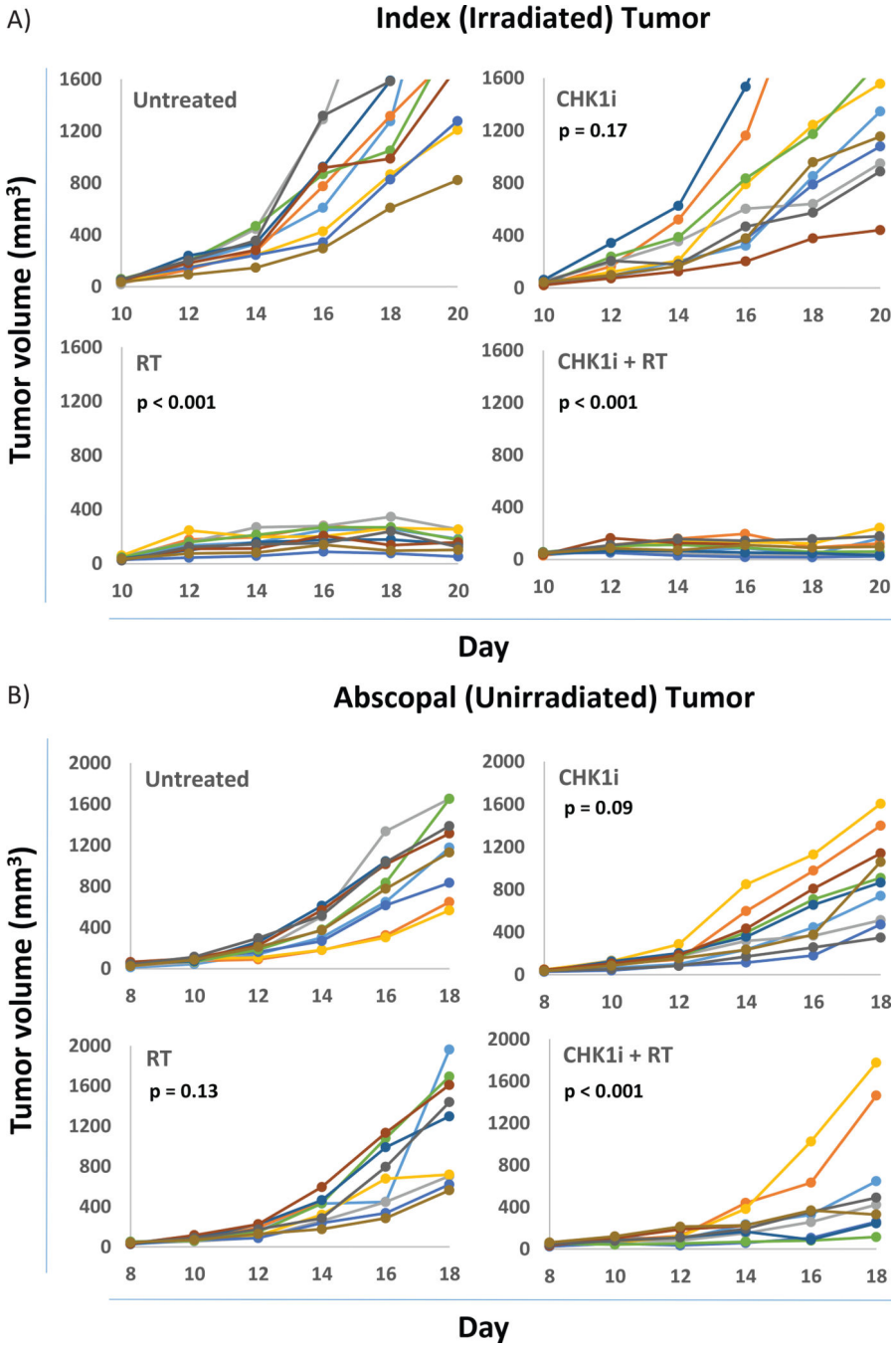

Figure 6: Tumor response in implanted B16-F10 tumors

A) Individual primary tumor responses for mice by treatment group (untreated, RT (17 Gy), CHK1i (AZD7762), CHK1i (AZD7762)+RT). B) Individual abscopal tumor responses for mice by treatment group. p-values shown are by log-rank test for tumor progression are in comparison to the untreated tumor group (see Statistical analyses in Methods).

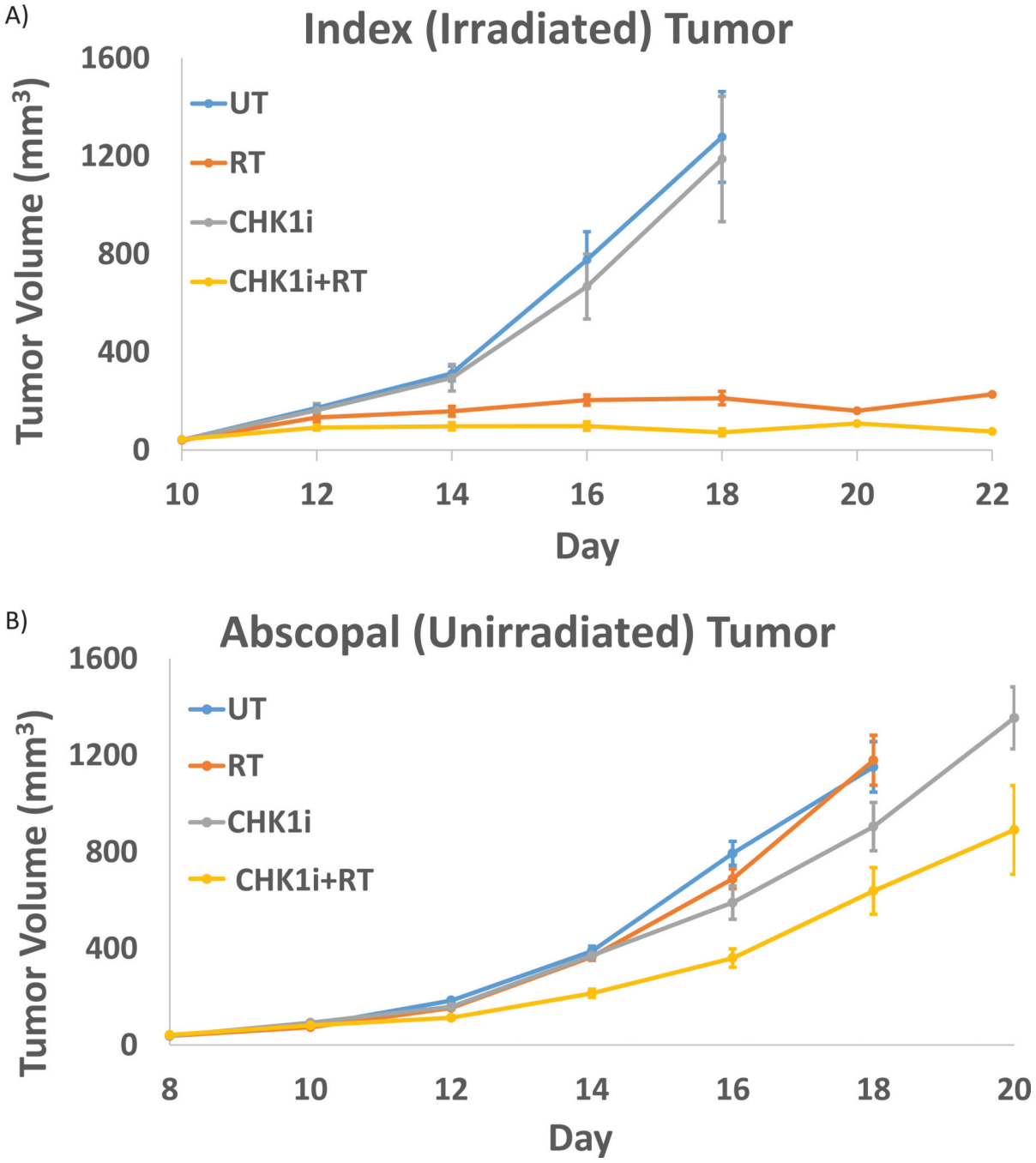

Figure 7: Tumor volume in implanted B16-F10 tumors

A) Average tumor volume of the primary tumor by treatment condition over time for each treatment group (untreated, RT (17 Gy), CHK1i (AZD7762), CHK1i (AZD7762) +RT). B) Average tumor volume of the abscopal tumor by treatment condition over time for each treatment group.

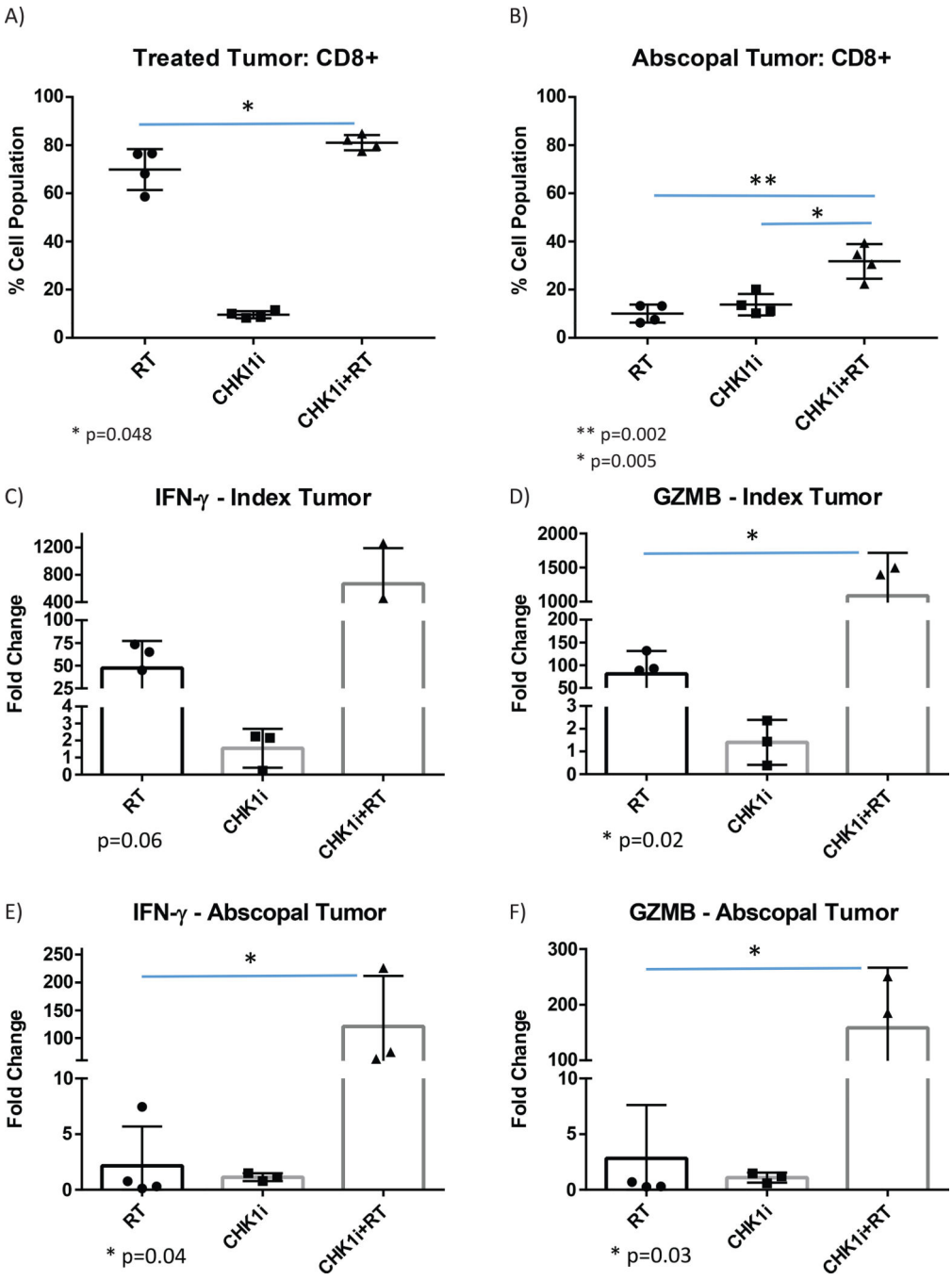

Figure 8: Immune activation by CD8 T-cell recruitment and gene expression in implanted B16-F10 tumors

A,B) Flow-assisted cell sorting analysis results indicating the activated CD8 T-cell population within B16-F10 tumors harvested 13 days following irradiation. Results for each treatment condition are shown in the A) primary irradiated tumor and B) abscopal unirradiated tumor.

C,D) Relative mRNA levels of B16-F10 tumors harvested 13 days following irradiation for the primary irradiated tumor by treatment condition (RT: n=4, CHK1i (AZD7762): n=3, CHK1i (AZD7762)+RT: n=3) for C) *IFN-γ*, and D) *GZMB.*

E,F) Relative mRNA levels of B16-F10 tumors harvested 13 days following irradiation for the abscopal unirradiated tumor by treatment condition (RT: n=4, CHK1i (AZD7762): n=3, CHK1i (AZD7762)+RT: n=3) for E) *IFN-γ*, and F) *GZMB*.

Values represent the mean ±S.D. of experimental replicates as shown; *, $P \leq 0.05$.